Nanoscale

PAPER

View Article Online
View Journal | View Issue

Cite this: *Nanoscale*, 2024, **16**, 4197

Film before aggregates: an *operando* GISAXS study on electrochemically assisted surfactant assembly†

Gilles E. Moehl, *[a] Samuel D. Fitch,[a] Katarina Cicvarić,[c] Yisong Han,[b] Ruomeng Huang, [c] Jonathan Rawle, [d] Li Shao,[a] Richard Beanland,[b] Philip N. Bartlett, [a] Guy Denuault [a] and Andrew L. Hector *[a]

Received 11th October 2023,
Accepted 29th January 2024

DOI: 10.1039/d3nr05126a

rsc.li/nanoscale

The process of electrochemically assisted surfactant assembly was followed in real time by grazing incidence small angle X-ray scattering with the aim to deconvolute the formation of mesoporous silica film and unwanted porous particles. The X-ray technique proved to be useful for the characterisation of this process, as it takes place at a very dynamic, solid/liquid interface. This paper shows the electrochemically driven onset and evolution of silica/surfactant structures. Additional control experiments indicate the formation of vertically aligned structures without the use of an electric field, although it seems to be beneficial for increased pore ordering.

Introduction

Templating through surfactant assembly allows for the fabrication of porous materials which have uses in the realms of optics, electronics, electrochemistry and sensing devices.[1] A major field of interest lies within structured thin films. Evaporation induced surfactant assembly (EISA) relies on the formation of a structured film through the self-assembly of a surfactant/precursor (silica) network during solvent evaporation.[2,3] This sol–gel based process can be carried out on flat surfaces using spin coating, dip coating and inkjet printing and has led to significant advances in the field of mesoporous nanostructures.[4,5] Printing allows some selectivity regarding the regions of the substrate that will be covered with the film. The most common structures produced in 2D-hexagonal silica films have linear pores which are aligned parallel to the substrate, which inhibits the transport of material through the pores to the substrate surface. Pore alignment and morphology selection remain the most challenging tasks within this – in principle – simple technique.

In 2007 Walcarius *et al.* reported an electrochemical process which enables the formation of vertically aligned mesoporous silica structures.[6] Electrochemically assisted surfactant assembly (EASA) uses the application of a potential difference between two electrodes to induce the self-assembly of a cationic surfactant on a conductive substrate. The current flow during deposition results in the formation of hydroxide ions and a local change of pH from acidic to alkaline, which catalyses the condensation of silica species to form a mesostructured gel.[7] The procedure works on a variety of conductive substrates such as indium-tin oxide (ITO), gold, carbon, platinum, titanium nitride,[8] and even on non-conductive substrates using high electric fields.[9] For the deposition, a pre-hydrolysed solution of tetraethyl orthosilicate (TEOS) and cetyltrimethylammonium bromide (CTAB) in 1 : 1 ethanol/water at pH = 3 is used. A sufficiently negative potential applied to the working electrode is then needed to induce film formation through the local increase of pH at the electrode surface. As soon as the cathodic potential is applied, hemispherical micelles are thought to form on the electrode surface.[10–12] Due to the use of an ethanol/water mixture as medium, the hydrocarbon chains of the CTAB assemble inside the hemimicelles leaving the TEOS on their outside. With increasing time, the micelles form vertical channels. Following deposition, the surfactant is removed by calcination or solvent extraction, leaving a mesoporous film with vertically aligned pore channels. Interestingly, vertically aligned structures can be obtained below and above the critical micelle concentration (CMC).[7] The lattice parameter of CTAB derived silica structures ranges from *circa* 3.8 nm for C_{14}TAB to 5 nm for C_{24}TAB, where the structure expands when made with a longer surfactant (until reaching a plateau).[13]

One problem arising when using EASA is the formation of unwanted aggregates on the film. The electrochemically gener-

[a]*School of Chemistry, University of Southampton, SO17 1BJ, UK. E-mail: G.E.H.K.Moehl@soton.ac.uk, A.L.Hector@soton.ac.uk*
[b]*Department of Physics, University of Warwick, CV4 7AL, UK*
[c]*School of Electronics and Computer Science, University of Southampton, SO17 1BJ, UK*
[d]*Diamond Light Source Ltd, Harwell Science & Innovation Campus, Didcot, OX11 0DE, UK*

† Electronic supplementary information (ESI) available. See DOI: https://doi.org/10.1039/d3nr05126a

ated hydroxides not only drive polycondensation of silica at the electrode surface, but also in the bulk solution above. This effect was shown to be related to the choice of counterion as well as sol ageing time.[14,15] With increasing CTAB/TEOS concentrations it has been found that more surface aggregates are formed due to the enhanced gelation speed. A rotating disk setup can be used to circumvent the formation of surface aggregates by preventing bulk solution silica condensation, as shown by Vanheusden *et al.*[16] The same goal can be achieved using an AC potential in an electrolyte without added salt, maintaining low pH at longer distances from the surface.[17]

In this paper, results of *operando* grazing incidence small angle X-ray scattering (GISAXS) measurements during EASA of silica are presented. The technique has been used to follow the EISA process in the past as it provides a unique access to the structure formation process.[18,19] The development of the nanostructure with time is discussed with respect to the current understanding of the process. Special attention is given to the temporal structure of the EASA process, characterising the onsets of film and aggregate formation.

Table 1 Compositions of the silica sol used during the *operando* GISAXS experiment at DLS/I07

Short name	CTAB (mg)	OTAB (mg)	Mesitylene (μl)	Mesitylene : CTAB
A1	480	0	0	0 : 1
A2	480	0	17.9	0.1 : 1
A3	480	0	90	0.5 : 1
A4	480	0	179	1 : 1
B1	0	480	0	0 : 1
B2	0	480	90	0.5 : 1
B3	0	480	179	1 : 1
B4	0	480	358	2 : 1

Results and discussion

Operando GISAXS measurements were carried out (60 s deposition + 24 s post deposition) during deposition of silica films onto TiN substrates at a potential of −2 V *vs.* Ag/AgCl for 60 s (Table 1, sol A1: $NaNO_3$, TEOS, CTAB in 1 : 1 H_2O/EtOH, pH = 3).[8] The current transients were similar to those obtained previously in EASA depositions (Fig. S1†). Prior to the application of the potential, no GISAXS signal apart from the background from the substrate is seen (Fig. S2a†), but a strong ring is visible at the end of deposition (Fig. S2b†). The first signal of the silica structure emerges at about 3 s into the deposition (Fig. 1a). Weak spots on either side of the specular reflection close to 1.7 nm^{-1} are visible as a small peak in the horizontal projection of the signal (Fig. 1d). About half a second later, this peak increases strongly in intensity and the ring signal becomes slowly visible (Fig. 1b and e), and continues to increase (Fig. 1c and f), as indicated by the red (spots) and yellow arrows (ring). This aligns with findings by Robertson *et al.*, who made vertically aligned films using EASA with deposition times shorter than 5 s and subsequent rinsing to avoid aggregate formation.[8]

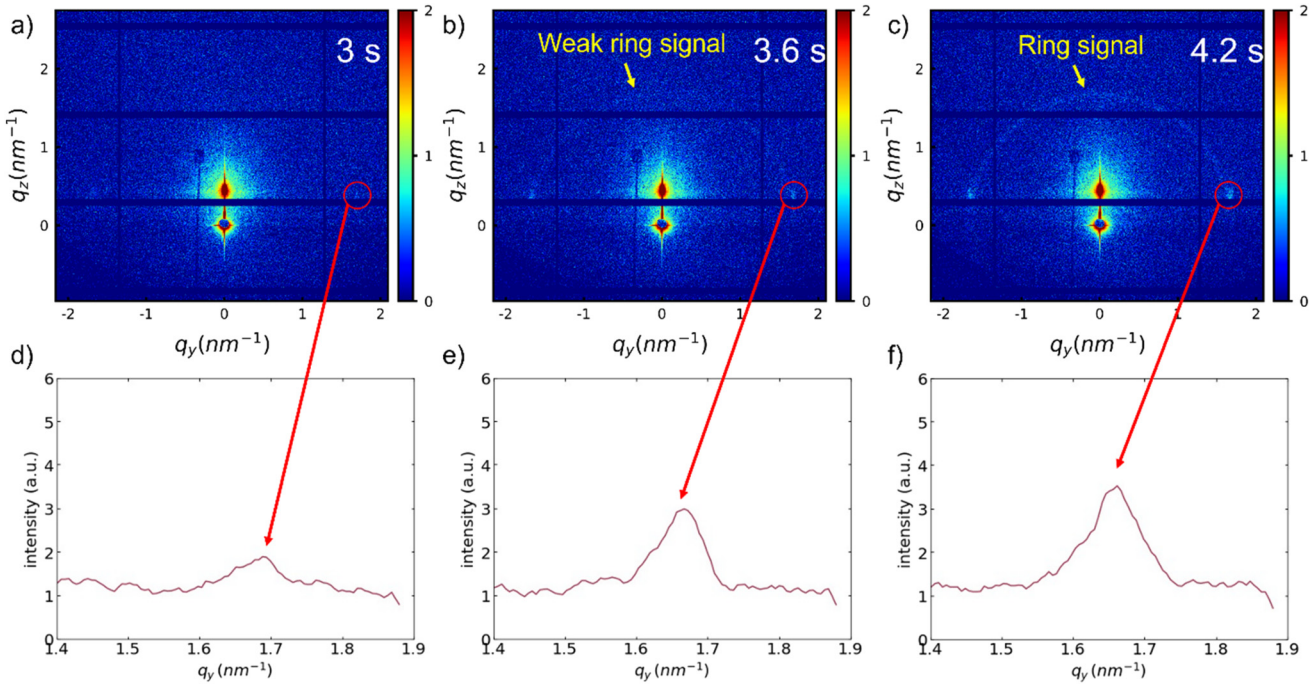

Fig. 1 Emergence of the first scattering features during silica deposition: (a) horizontal spots appear (compact film, vertical alignment), (b) spots increase in intensity and ring becomes visible, (c) both signals fully visible. (d–f) Horizontal integrations of the spot signals for the detector images shown in (a–c) respectively at q_z = 0.5 nm^{-1}.

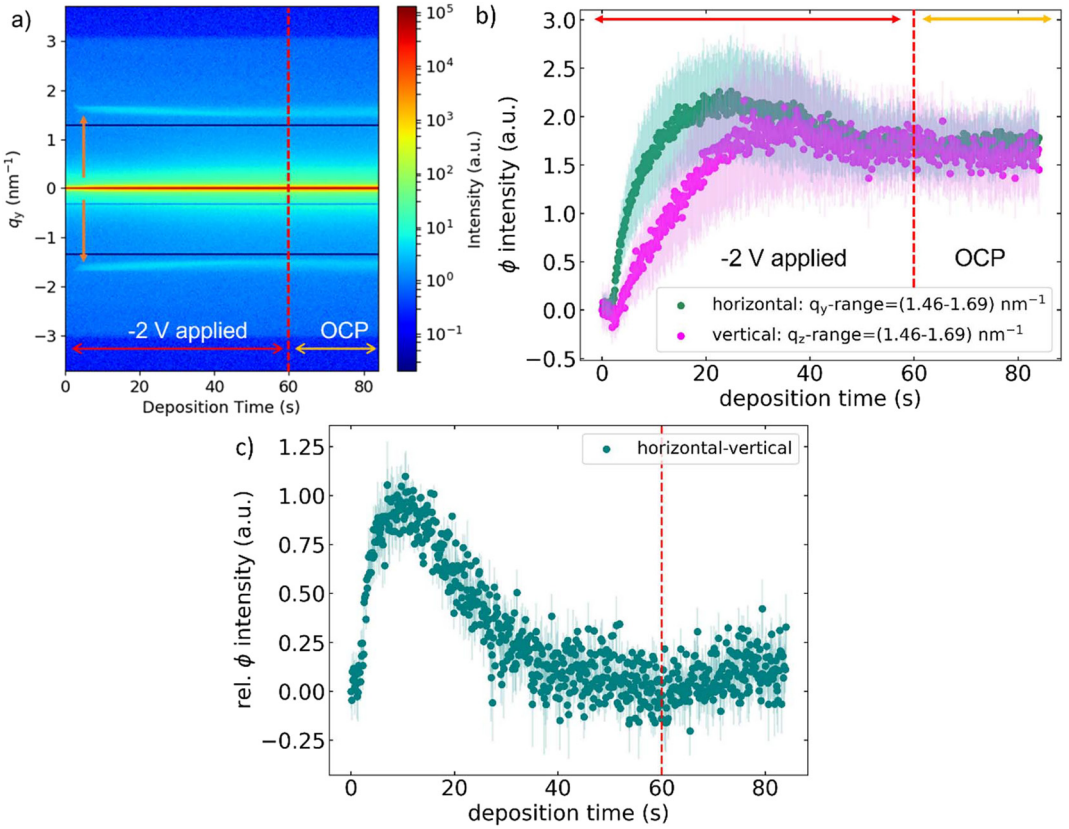

Fig. 2 (a) Contour plot of horizontal scattering profiles extracted from each frame *versus* deposition time. Integrations were performed at the Yoneda position of the TiN/silica sol interface at q_z = 0.5 nm^{-1}. The blue line below q_y = 0 is the shadow of the beam stop that was not used in this experiment but kept close to its working position because it would not move reliably over large distances. The two symmetrical dark lines outside of q_y = ±1.0 nm^{-1} are detector gaps. (b) Intensity of the averaged signal in the q_y (green, q_z = 0.5 nm^{-1}) and q_z (fuchsia, q_y = 0) range between 1.46 and 1.7 nm^{-1} *vs.* deposition time during EASA using CTAB with error bars (light green, light fuchsia). (c) Subtraction of the curves shown in (b) (horizontal−vertical).

Fig. 2(a) shows a contour plot of the horizontal scattering profiles extracted from each frame *versus* deposition time at q_z = 0.5 nm^{-1}. The features around 1.62 nm^{-1} along the lateral direction appear in the scattering images after 3 s, which then symmetrically move towards smaller q_y values until the end of the potential step at 60 s where the working electrode returned to OCP. GISAXS data were recorded until 85 s and show that after 60 s, q_y values slightly increase again. The peak position of the features was extracted using custom-made Python based software.

Fig. 2(b) shows the change with time of the horizontal (q_z = 0.5 nm^{-1}) as well as vertical (q_y = 0) intensity averaged over the q-range 1.46–1.7 nm^{-1} (both zeroed to respective initial background signal) showing a sharp increase after a few seconds when silica condensation starts, with a maximum around 22 s and a plateau after 40 s. The formation of SiO_2 increases the contrast between the solid parts of the film and the solution environment, leading to the increase in intensity soon after applying the potential. In addition, the highly ordered assembly of the surfactant also contributes to this increase due to the generation of coherent scattering from its structure. The horizontal signal increases prior to the vertical one, with a higher rate. This proves the formation of a vertically aligned structure in addition to the isotropically oriented pores within the aggregates. Subtraction of the apparent intensities (horizontal minus vertical) (see Fig. 2(c)) enlightens this further. The data shows an intensity peak at about 12 seconds. This could mean that the ordering process of the vertically aligned pores finished just after 10 seconds of deposition. Fig. 3(a) shows the changing position of the GISAXS peaks during silica deposition. Peak positions (blue: spot, purple: ring) were extracted by fitting a twin Gaussian function to the GISAXS peaks in each frame (700 in total), where one position corresponds to the spot and one to the ring feature. The position of the spot is at slightly higher q_y-value than the ring, as discussed in more detail later. The decreasing magnitude of the q_y-values corresponds to an increasing d-spacing during deposition which is associated with the inflation of the structure. This continues until reaching 40 s deposition time, at which point the curve reaches a plateau at q_y = 1.56 nm^{-1} lasting up to 60 s, where the potential is switched to OCP. After that, the q_y-values slightly increase again until the end of the measurement at 84 s. The inflation of the structure reaches its maximum shortly after the maximum in averaged intensity

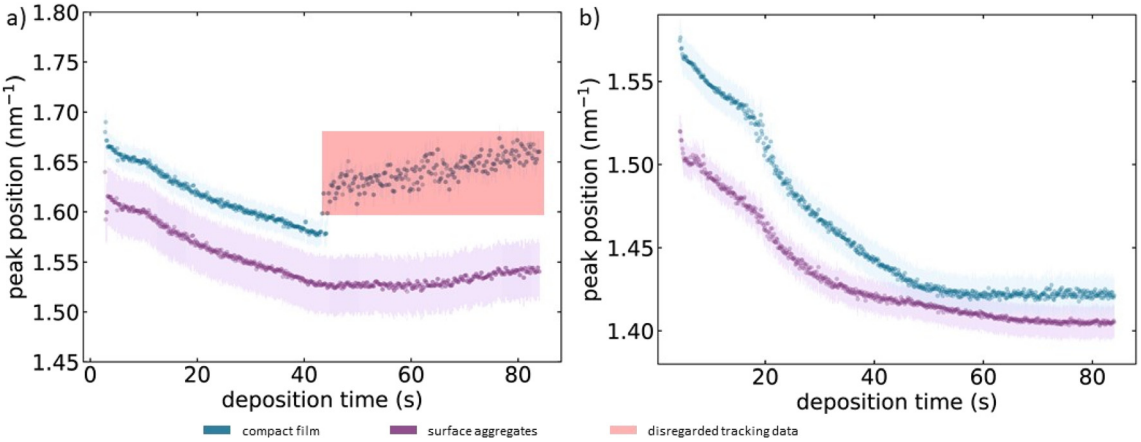

Fig. 3 Position of the horizontal peaks (blue: spot, purple: ring) *vs.* deposition time during EASA using (a) CTAB and (b) OTAB as the surfactant. Peak positions were extracted from individual Gaussian fits of the peaks within horizontal profiles taken at q_z = 0.5 nm^{-1} in each frame (700 in total).

(previously) shown in Fig. 2(b). At this point, the contrast between silica structure and solution reaches its highest value, which might correspond to crossing the gel-point of the system. This assumes that the solid silica parts of the gel have the highest electronic density in the system, leading to the highest scattering contrast when transitioning from sol to gel, but does not take into account the contributions from increased ordering in the structure to the amount of coherent scattering. The network is sufficiently solid to retain the pore spacing, although a slight shrinkage is observed through the increasing q-value. Beyond 22 s, the reduction of the TiN area by the growing silica structure limits hydroxide generation and, consequently, the condensation process. When comparing this profile to the current transients in Fig. S1,† one can see that the electrochemistry does not directly reflect any of the features seen in the scattering data. When applying the constant potential, a sudden increase in current can be observed (sub-second response time), which corresponds to the formation of an electrochemical double layer, followed by the reduction of water to H_2 and $[OH]^-$ due to the rather low potential. The faradaic current then plateaus off when reaching a steady diffusion current, but at 3 s there is no direct feature indicating surfactant assembly in the transient profile.

The "inflation" of the structure shown in Fig. 3(a) (decrease in peak position) could arise from hydroxide ions generated at the electrode surface which, due to electrostatic repulsion with the negatively charged silica walls, make the structure swell as they diffuse through. The trend matches the deflation of the structure (shift in peak position) observed as soon as the potential is switched off and left at OCP. Another possibility could be that the expansion process is related to the diffusion of ethanol, produced during the condensation of TEOS, into the micelles.[20] This effect is expected to decrease the overall curvature of the micelles formed on the electrode surface, ultimately leading to their elongation into standing pore channels. The sol consists of ethanol and water in equal amounts, which means the ethanol global concentration cannot massively change as a result from this reaction.

The same experimental procedure was applied to a sol containing octadecyltrimethylammonium bromide (OTAB) instead of CTAB (sol B1 in Table 1). The electrochemical data can be seen in Fig. S1(b).† The transient has the same shape as the one obtained in the CTAB experiment. The elongation of the chain from 16 to 18 carbon atoms was expected to result in a slightly enlarged pore distance.[13] Once again, a contour plot of the horizontal scattering profiles was made, as shown in Fig. S4.† Note the close association of the randomly appearing lines in the contour plots with a vibration of the beamstop during the experiment, which led to overexposure of the detector in some frames, but otherwise did not have any impact on the data treatment as the signal of interest was always clearly visible. The scattering signal has a very similar appearance to the one shown in the CTAB experiment (see Fig. 2a), with symmetrical peaks appearing a few seconds after switching on the potential, migrating towards smaller q_y values until 60 s, after which a slight increase is observed. Even to the naked eye, the peak position shift to smaller q_y values is noticeable. The scattering profiles were once again fitted using a twin peak function consisting of two Gaussian peaks, as shown in Fig. 3(b) (blue: spot, purple: ring). As expected, the peak positions are generally shifted to smaller q_y-values due to the longer chain length of OTAB, but the inflation effect prevails. The experiment shows that a slight elongation of the surfactant chain leads indeed to a larger pore structure, and that the swelling effect remains due to the otherwise identical conditions of the reaction.

In the second part of the study, the swelling agent mesitylene was added to the silica sols (see ESI†). The hydrophobic molecule was added to the system in order to increase the diameter of the micelles, which results in increased pore size and spacing of the silica structure.[8] The experiments show that the previously described behaviour of the system is maintained when adding the swelling agent, hence the detailed discussion of this data is presented in the ESI.†

To verify the assumption that a compact film was formed under a thick layer of aggregates, further characterisation was

needed. After each experiment (84 s in total), the sample was pulled from the sol. For this, the cell was flushed with ethanol using the peristaltic pumps connected to the cell. The surfactant was removed from samples by immersion into 0.2 M HCl in ethanol for at least 5 minutes, after which it was cleaved for cross-sectional analysis by SEM (*post mortem*). Fig. 4(a) shows a very thick layer of piled up spherical aggregates (total thickness *circa* 30 μm), on top of the film. Fig. 4(b) clearly reveals the structure of the sample which consists, from bottom to top, of the silicon substrate, the TiN layer, a compact silica layer, and the surface aggregates. This explains the features seen in Fig. 1: the spots correspond to the compact layer of silica (first order peak of the P_6mm 2D hex structure); the ring to the surface aggregates. Spots in the horizontal direction of a GISAXS pattern indicate a vertically aligned structure, while the ring is the result of the porous aggregates not having any preferred pore orientation.

With EASA being a highly dynamic process, following the reaction in real-time allows us to compare the data with postulations around the mechanism, which are mainly based on the *post mortem* analysis of thin films. Parts of this discussion can be found in our previous publication,[17] in which we showed that under conditions with oscillating potential, vertically aligned films could be formed on the substrate. We concluded that the requirement for vertical pore alignment is sufficient supply of hydroxide species near the electrode surface, seemingly independent of its apparent potential. This discussion will now be resumed in the following section.

The GISAXS data show that after an initial delay time, a vertical structure arises, almost immediately followed by the formation of surface aggregates (Fig. 1). The delay corresponds to the time needed for homogeneous gelation (aggregate formation) calculated by Liu *et al.*[21] We have postulated before that heterogeneous gelation should represent a lower limit of the reaction time, at which sufficient reactive species are present to form the compact film.[17] The GISAXS measurements confirm this due to the emergence of the film signal (spots) prior to the aggregate signal (ring). This also supports the findings of Vanheusden *et al.* and our previously published work,[16,17] which essentially make use of this effect to generate aggregate free films by excluding the condition of homogeneous gelation.

The literature consistently argues that the electric field present during EASA is the main reason why the pore channels align vertically instead of horizontally to the surface, because it is the major difference to EISA based procedures. In addition, Guillemin *et al.* reported that only a negatively charged substrate led to the formation of vertically aligned pores in an experiment where silica microdots were generated using a microelectrode.[22] When reversing the potential and using the microelectrode as working electrode, only disordered silica was found on the substrate (in this case counter electrode), which was taken as indication for the importance of polarity, but using opposing pH gradients. Stöber-growth on silica surfaces also produces vertically aligned pores, with no electric field present.[23] This was reason enough to conduct a number of control experiments, probing the effect of the electric potential.

The surfactant in a silica free solution was investigated first: immersing a blank TiN substrate into a solution of 0.1 M $NaNO_3$/EtOH (1 : 1) with CTAB (480 mg per 20 ml water) for two minutes results in the formation of a horizontally aligned structure, as shown in Fig. S7.† The first order peak around 2.4 nm^{-1} corresponds to an interlayer thickness of 2.6 nm, which lies within the range of the length of CTA^+ surfactant cations.[24] The procedure was repeated while applying a potential to the blank TiN electrode, which led to the same horizontally-aligned structure (not shown), implying that the potential does not affect the CTAB self-assembly. This is in agreement with previous reports,[11,12] where CTAB was shown to form either a lamellar monolayer (headgroups on both sides, tails inside with strong intermixing), or a flat layer with hemimicelles on top. Our experiments show that, even though CTAB is a cationic surfactant, it does not react to the application of a potential to the electrode (at least not visibly in this experiment), or in other words: in this scenario, there is no visible difference when momentarily applying a potential. This means any processes happening under static electric potential at the

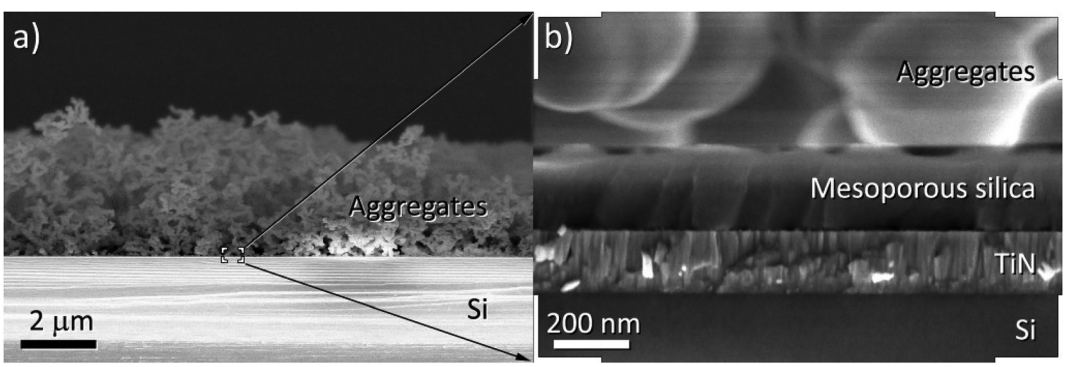

Fig. 4 (a) SEM cross-sections of sample A1. (b) (Zoom into a) The bottom of the images shows the Si substrate, with the 200 nm thick TiN layer on top, which in turn is covered by a layer of mesoporous silica with roughly the same thickness. On the very top, spherical aggregates can be seen, which form a layer up to 5 microns thick. Surfactant was removed prior to microscopy by immersion into 0.2 M HCl in ethanol for 5 minutes.

electrode are not visible in this study and might be worthwhile to investigate in the future.

To further test this observation, another experiment was conducted where a TiN substrate was immersed in the previously mentioned "dummy sol" for a couple of minutes, after which first 905 μl of TEOS (per 20 ml water) were added, followed by 12 μl (per 20 ml of water) of 35 wt% NH_3 solution. The rationale behind this was to emulate the conditions during EASA, without applying a potential to the electrode, which is why ammonia solution was used to induce the change in pH from acidic to alkaline. The substrate was left without stirring overnight and recovered the next day. A corresponding GISAXS image is shown in Fig. S8.† A vertically aligned structure of typical dimension was obtained (spots), including surface aggregates (ring).

This proves that the replication of the EASA conditions without any electric field lead to a very similar result in terms of the pore alignment. This does not mean that there generally are no interactions between surfactant, silica species and polarised surfaces, but their individual mechanisms cannot be distinguished in this work. The electric field is shown not to be necessary for the vertical assembly of the micelles, although it does result in a greater level of hexagonal ordering of the pore network. The observation is very similar to the behaviour observed in polyelectrolyte/surfactant systems at the water/air interphase, where silica takes the role of a polyelectrolyte.[25] The difference however is, that those films do not align vertically to the interphase. Using the target surface as the source of catalysts needed for the reaction is advantageous to the simple incorporation by stirring, making EASA a faster and more selective route for the making of mesoporous silica films.

Conclusions

The major point of interest in this work is the formation of mesoporous silica films through EASA. The process was monitored in real-time using GISAXS, showing that a compact film with vertically aligned pores as well as mesoporous surface spherical aggregates that form shortly after the film and on top of it. Individual integrations of the horizontal and vertical scattering signals can be used to delineate the formation of the vertically aligned structure as well as the isotropic structure due to the random orientation of the ordered hexagonal pores in the surface aggregates. During application of the potential, the whole structure inflates slightly in size. This effect was present regardless of the employed surfactant/amount of swelling agent, although its degree varied depending on the conditions. A maximum in scattering contrast was seen on a similar time scale and was interpreted as an indication for passing the transition point of the system from sol to gel, after which the gel became too rigid to undergo any further changes in pore spacing. Limitations of pore swelling were seen with increasing amounts of mesitylene for both employed surfactants, indicating that the swelling agent undergoes a transition from co-surfactant to co-solvent, the critical concentration of which seems to depend on the chain length of the surfactant. In control experiments, pore alignment in the compact films was not found to be dependent on the electric field, as vertically ordered structures could be generated in its absence using similar conditions. For future studies, GISAXS could be used to very accurately optimise deposition protocols in solution, and to determine critical parameters of the system as *e.g.*, surface/bulk CMC of the surfactant in presence of the silica precursor.

Experimental

A variety of different solutions was used during the *operando* GISAXS-EASA experiment, as shown in Table 1. All solutions consisted of 20 ml 0.1 M $NaNO_3$ and 20 ml ethanol at pH = 3 (using 0.2 M HCl). Either hexadecyltrimethylammonium bromide (CTAB) or octadecyltrimethylammonium bromide (OTAB) were then used as surfactant and different amounts of mesitylene were used as swelling agent to increase the pore size of the network. Lastly, 905 μl of TEOS were added to the solution under stirring. Table 1 shows the different compositions of the solutions used with their short names. The dummy sol was made of only 20 ml 0.1 M $NaNO_3$ and 20 ml ethanol at pH = 3 (using 0.2 M HCl).

The presented *operando* experiments were carried out at Diamond Light Source using beamline I07. A custom-made PEEK (polyether ether ketone) cell was used, of which a schematic drawing is shown in Fig. S9.† It consists of two outer PEEK elements, which mechanically hold Kapton foil onto the inner part (with O-rings), effectively working as water tight X-ray windows. TiN sputtered on Si wafer was used as the working electrode (5 × 10 mm^2 active area), Pt gauze as the counter and Ag/AgCl as the pseudo reference. Working and counter electrodes were placed opposite to each other in parallel for homogeneous deposition. During the deposition of silica through the application of −2 V for 60 s (Biologic SP-150 potentiostat), scattering images were recorded using a Dectris Pilatus 2M detector with 100 ms exposure time and 20 ms readout. In total, 700 images were recorded for each experiment, leading to a total time of 84 s. Silver behenate (AgBh) was used to accurately measure the sample detector distance of 2007.52 mm using the calibration tool in the software DPDAK.[26] The potential was switched off 60 s after the start of scattering data acquisition, meaning that GISAXS images were recorded until 24 s after this point. After the complete assembly of the cell, the respective solution was pumped through the cell using a peristaltic pump (Ismatec) in order to fill it up and the flow was maintained throughout the alignment and measurement. It was then mounted onto the beamline's hexapod with a custom-made cell holder. Sample alignment was done using a standard procedure: at first the height was scanned using the direct beam and then adjusted to half-cut conditions. Then, the incident angle was scanned until a reflection from the sample surface was obtained. From the

pixel position of the reflections on the detector, the zero position was extrapolated by a linear fit of angle *vs.* specular intensity. The whole procedure was repeated once in order to ensure precise alignment conditions. The critical angle of TiN at 12.25 keV has a value of 0.21°, so 0.20° was used as the incident angle for the experiments in order to probe the whole film above the substrate, since the TiN surface is totally reflecting in this setting. The sample detector distance was set in a way that the first order peak of the silica structure which resides typically around 1.6 nm^{-1} would be at the centre of the q_y range, giving enough probed q_y-space on both sides to enable detection of smaller as well as much larger structures.

In order to make sure the *operando* GISAXS cell would provide equivalent electrochemical conditions to those typically used for the EASA of silica, control experiments were done in house, using the exact same electrochemical setup. The scattering image was then recorded in house on our Rigaku Smartlab system (sample detector distance: 301 mm, wavelength: 1.54 Å). Deposition times were kept in the range of seconds only in order to minimize the formation of surface aggregates so that the presence of vertically aligned channels could be confirmed. Fig. S10(a)† shows the corresponding SEM and Fig. S10(b)† GISAXS image of a silica deposited onto TiN using a potential of −2.0 V for the duration of 2 s. Only a small number of aggregates can be seen in the microscopy, and the GISAXS clearly shows two spots in horizontal direction, corresponding to vertically aligned pore channels. A very slight ring can be seen too, due to the presence of a few surface aggregates.

Author contributions

G. M. and A. H. designed the experimental study. K. C. and R. H. provided TiN substrates. G. M., L. S., S. F., J. R. and A. H. performed the GISAXS experiments. G. M. analysed the data. Y. H. and R. B. performed the SEM measurements. G. M., A. H. and G. D. wrote the original draft. G. M., S. F., K. C., Y. H., R. H., J. R., L. S., R. B., P. B., G. D, and A. H. edited and revised the manuscript draft.

Conflicts of interest

There are no conflicts to declare.

Acknowledgements

This work has been supported by EPSRC through the Advanced Devices by Electroplating Program grant (ADEPT; EP/N035437/1) and through equipment funding (EP/K00509X/1 and EP/K009877/1). Synchrotron beam time was provided by Diamond Light Source, beamline I07 under experiment si20593-1. The authors would like to thank the I07 beamline staff for excellent support and data quality.

References

1 L. Nicole, C. Boissière, D. Grosso, A. Quach and C. Sanchez, *J. Mater. Chem.*, 2005, **15**, 3598–3627.
2 Y. Lu, R. Ganguli, C. A. Drewien, M. T. Anderson, C. Jeffrey Brinker, W. Gong, Y. Guo, H. Soyez, B. Dunn, M. H. Huang and J. I. Zink, *Nature*, 1997, **389**, 364–368.
3 C. J. Brinker, *MRS Bull.*, 2004, **29**, 631–640.
4 D. Grosso, F. Cagnol, G. J. de A. A. Soler-Illia, E. L. Crepaldi, H. Amenitsch, A. Brunet-Bruneau, A. Bourgeois and C. Sanchez, *Adv. Funct. Mater.*, 2004, **14**, 309–322.
5 C. J. Brinker, Y. Lu, A. Sellinger and H. Fan, *Adv. Mater.*, 1999, **11**, 579–585.
6 A. Walcarius, E. Sibottier, M. Etienne and J. Ghanbaja, *Nat. Mater.*, 2007, **6**, 602–608.
7 A. Walcarius, J. Ghanbaja, M. Etienne, E. Aubert, C. Lecomte and A. Goux, *Chem. Mater.*, 2009, **21**, 731–741.
8 C. Robertson, R. Beanland, S. A. Boden, A. L. Hector, R. J. Kashtiban, J. Sloan, D. C. Smith and A. Walcarius, *Phys. Chem. Chem. Phys.*, 2015, **17**, 4763–4770.
9 A. Walcarius, *Chem. Soc. Rev.*, 2013, **42**, 4098–4140.
10 A. E. Sánchez-Rivera, M. Romero-Romo, M. T. Ramírez-Silva, M. Palomar-Pardavé and V. Vital-Vaquier, *J. Electrochem. Soc.*, 2004, **151**, C666.
11 R. K. Lee, E. M. Simister and E. A. Thomas, *Langmuir*, 1990, **6**, 1031–1034.
12 J. F. Liu and W. A. Ducker, *J. Phys. Chem. B*, 1999, **103**, 8558–8567.
13 N. A. N. Mohamed, Y. Han, A. L. Hector, A. R. Houghton, E. Hunter-Sellars, G. Reid, D. R. Williams and W. Zhang, *Langmuir*, 2022, **38**, 2257–2266.
14 E. Sibottier, S. Sayen, F. Gaboriaud and A. Walcarius, *Langmuir*, 2006, **22**, 8366–8373.
15 Y. Guillemin, J. Ghanbaja, E. Aubert, M. Etienne and A. Walcarius, *Chem. Mater.*, 2014, **26**, 1848–1858.
16 G. Vanheusden, H. Philipsen, S. J. F. Herregods and P. M. Vereecken, *Chem. Mater.*, 2021, **33**, 7075–7088.
17 G. E. Moehl, T. Nasir, Y. Han, Y. J. Noori, R. Huang, R. Beanland, P. N. Bartlett and A. L. Hector, *Nanoscale*, 2022, **14**, 5404–5411.
18 D. Grosso, F. Babonneau, G. J. de A. A. Soler-Illia, P.-A. Albouy and H. Amenitsch, *Chem. Commun.*, 2002, 748–749.
19 B. Platschek, R. Kóhn, M. Dóblinger and T. Bein, *ChemPhysChem*, 2008, **9**, 2059–2067.
20 C. J. Brinker and G. W. Scherer, *Sol-Gel Science, The Physics and Chemistry of Sol-Gel Processing*, Academic Press, 1990.
21 L. Liu and A. Walcarius, *Phys. Chem. Chem. Phys.*, 2017, **19**, 14972–14983.
22 Y. Guillemin, M. Etienne, E. Sibottier and A. Walcarius, *Chem. Mater.*, 2011, **23**, 5313–5322.
23 X. Zhang, Y. Dou, C.-Y. Mou, A. M. Asiri, Z. Teng, W. Li, G. Zheng and D. Zhao, *Angew. Chem., Int. Ed.*, 2012, **51**, 2173–2177.

24 N. V. Venkataraman and S. Vasudevan, *Proc. Indian Acad. Sci.: Chem. Sci.*, 2001, **113**, 539–558.
25 K. J. Edler, A. Goldar, T. Brennan and S. J. Roser, *Chem. Commun.*, 2003, 1724–1725.
26 G. Benecke, W. Wagermaier, C. Li, M. Schwartzkopf, G. Flucke, R. Hoerth, I. Zizak, M. Burghammer, E. Metwalli, P. Müller-Buschbaum, M. Trebbin, S. Förster, O. Paris, S. V. Roth and P. Fratzl, *J. Appl. Crystallogr.*, 2014, **47**, 1797–1803.